
Kinetic Analysis of ^{18}F -Fluorodihydrorotenone as a Deposited Myocardial Flow Tracer: Comparison to ^{201}Tl

Robert C. Marshall, MD; Patricia Powers-Risius, BA; Bryan W. Reutter, MS; James P. O'Neil, PhD; Michael La Belle, PhD; Ronald H. Huesman, PhD; and Henry F. VanBrocklin, PhD

Department of Nuclear Medicine and Functional Imaging, E.O. Lawrence Berkeley National Laboratory, University of California, Berkeley, California

The goals of this investigation were to assess the accuracy of ^{18}F -fluorodihydrorotenone (^{18}F -FDHR) as a new deposited myocardial flow tracer and to compare the results to those for ^{201}Tl .

Methods: The kinetics of these flow tracers in 22 isolated, erythrocyte- and albumin-perfused rabbit hearts were evaluated over a flow range encountered in patients. The 2 flow tracers plus a vascular reference tracer (^{131}I -albumin) were introduced as a bolus through a port just above the aortic cannula. Myocardial extraction, retention, washout, and uptake parameters were computed from the venous outflow curves with the multiple-indicator dilution technique and spectral analysis. **Results:** The mean \pm SD initial extraction fractions for ^{18}F -FDHR (0.85 ± 0.07) and ^{201}Tl (0.87 ± 0.05) were not significantly different, although the initial extraction fraction for ^{18}F -FDHR declined with flow ($P < 0.0001$), whereas the initial extraction fraction for ^{201}Tl did not. The washout of ^{201}Tl was faster ($P < 0.001$) and more affected by flow ($P < 0.05$) than was the washout of ^{18}F -FDHR. Except for the initial extraction fraction, ^{18}F -FDHR retention was higher ($P < 0.001$) and less affected by flow ($P < 0.05$) than was ^{201}Tl retention. Reflecting its superior retention, the net uptake of ^{18}F -FDHR was better correlated with flow than was that of ^{201}Tl at both 1 and 15 min after tracer introduction ($P < 0.0001$ for both comparisons). **Conclusion:** The superior correlation of ^{18}F -FDHR uptake with flow indicates that it is a better flow tracer than ^{201}Tl in the isolated rabbit heart. Compared with the other currently available positron-emitting flow tracers (^{82}Rb , ^{13}N -ammonia, and ^{15}O -water), ^{18}F -FDHR has the potential of providing excellent image resolution without the need for an on-site cyclotron.

Key Words: myocardial perfusion; ^{18}F -fluorodihydrorotenone; PET

J Nucl Med 2004; 45:1950–1959

Incomplete extraction and retention of ^{201}Tl - and $^{99\text{m}}\text{Tc}$ -labeled flow tracers contribute to diagnostic and prognostic uncertainties in SPECT myocardial perfusion imaging (1–5). Although ^{82}Rb , ^{13}N -ammonia, and ^{15}O -water can be used with PET to assess myocardial perfusion (6–9), problems with image resolution or the need for an on-site cyclotron has discouraged their widespread use. In an effort to find better perfusion indicators, we have been evaluating radiolabeled rotenone compounds as deposited myocardial flow tracers. Rotenone is a neutral lipophilic compound that binds to complex I in the mitochondrial electron transport chain (10–13). Marshall et al. recently reported that ^{125}I -iodorotenone was superior to $^{99\text{m}}\text{Tc}$ -sestamibi as a deposited flow tracer in the isolated rabbit heart (14).

In this investigation, a second radiolabeled rotenone analog, ^{18}F -fluorodihydrorotenone (^{18}F -FDHR), was evaluated as a potential myocardial flow tracer and was compared to ^{201}Tl instead of $^{99\text{m}}\text{Tc}$ -sestamibi. The experimental preparation was the isolated, isovolumic rabbit heart perfused retrograde with red blood cells (RBC) and bovine serum albumin (BSA). ^{18}F -FDHR and ^{201}Tl kinetics were assessed at flow rates ranging from 0.3 to 3.5 mL/min/g of left ventricular (LV) wet weight. Myocardial tracer deposition was determined from venous outflow curves after bolus introduction of ^{18}F -FDHR, ^{201}Tl , and the intravascular tracer ^{131}I -albumin. Initial extraction fraction, net retention, washout, and net uptake of both flow tracers were computed with the multiple-indicator dilution technique and spectral analysis (14–16). Spectral analysis allowed separation of extravascular from intravascular tracer distributions and was also used in a previous report comparing ^{125}I -iodorotenone and $^{99\text{m}}\text{Tc}$ -sestamibi (14). Because the experimental protocols and data analyses were identical in these 2 studies, it is possible to compare the results for all 4 flow tracers.

The results of this study indicate that ^{18}F -FDHR and ^{201}Tl were equally well extracted during the initial peak of the venous outflow curves. However, net retention and net uptake of ^{18}F -FDHR were higher than those of ^{201}Tl for the

Received Mar. 19, 2004; revision accepted Jul. 15, 2004.

For correspondence or reprints contact: Bryan W. Reutter, Department of Nuclear Medicine and Functional Imaging, E.O. Lawrence Berkeley National Laboratory, University of California, 1 Cyclotron Rd., MS55-121, Berkeley, CA 94720.

E-mail: bwreutter@lbl.gov

remainder of the 15-min experiment, making ^{18}F -FDHR superior to ^{201}Tl as a deposited flow tracer in the isolated rabbit heart. When the results of both studies were compared, the 2 radiolabeled-rotenone analogs had first-pass extraction fractions comparable to that of ^{201}Tl and better retention than $^{99\text{m}}\text{Tc}$ -sestamibi for at least 15 min after tracer introduction, making ^{18}F -FDHR and ^{125}I -iodorotenone better flow tracers in the isolated rabbit heart. If similar results are observed in patients, ^{123}I -rotenone could be used with SPECT and ^{18}F -FDHR could be used with PET for a more accurate assessment of regional myocardial perfusion during stress and at rest.

MATERIALS AND METHODS

Experimental Preparation

All procedures were performed according to institutional guidelines for animal research. Isovolumic, retrograde RBC- and albumin-perfused rabbit hearts ($n = 22$) were prepared in a manner similar to that in previous reports (14,17). Hearts were obtained from male New Zealand White rabbits (R&R Rabbitry) weighing approximately 4 kg. The perfusate buffer was modified Tyrode's solution containing BSA at 22 g/L (fraction V, fatty-acid free; Roche Diagnostics) and oxygenated bovine RBCs adjusted to a hematocrit level of 17%–20%. Substrates were glucose at 5 mmol/L and sodium pyruvate at 2 mmol/L. Electrolyte concentrations were 110 mmol/L for NaCl, 2.5 mmol/L for CaCl_2 , 6 mmol/L for KCl, 1 mmol/L for MgCl_2 , 0.435 mmol/L for NaH_2PO_4 , and 28 mmol/L for NaHCO_3 . The pH and oxygen tensions were measured with an IRMA blood gas analyzer (Diametrics Medical, Inc.). The mean \pm SD pH was 7.44 ± 0.06 , and the partial pressure of oxygen was 320 ± 127 mm Hg. To maintain oxygenation and a stable pH, the surface of the RBC-containing perfusate was equilibrated with a mixture of 98% O_2 and 2% CO_2 during the experiment.

After a rabbit was given 4,000 U of heparin (Upjohn) and 250 mg of pentobarbital sodium (Abbott) through an ear vein, the heart was excised through a median sternotomy, arrested in ice-cold saline, and attached to a cannula to allow retrograde perfusion. After an apical drain was inserted into the left ventricle, a fluid-filled latex balloon connected to a Gould-Statham P231D pressure transducer (Gould) was inserted across the mitral valve into the LV cavity. Perfusion pressure and systolic and diastolic ventricular pressures were recorded continuously with a Linearecorder (Western Graphtec). A coronary venous sampling catheter and a needle thermistor (Omega Engineering, Inc.) were inserted into the right ventricular cavity across the tricuspid valve. The venae cavae and pulmonary artery were ligated so that all coronary venous drainage flowed out of the sampling catheter. The atrioventricular node was crushed to allow controlled stimulation by 4-V, 4-ms stimuli from an SD44 stimulator (Grass Medical Systems). Temperature was maintained between 36°C and 38°C with a water-jacketed heating coil and a heart chamber. Coronary flow was kept constant with a peristaltic pump (Rainin Instruments). The coronary blood flow rate was measured by timed collection from the venous sampling catheter. The perfusate was not recirculated. Hearts were allowed to equilibrate for 15 min after surgical preparation was complete. During equilibration, developed pressure (peak systolic minus diastolic) was stable and averaged 73 ± 14 mm Hg.

Experimental Protocol

After equilibration, myocardial perfusion was gradually changed to the experimental flow rate and subsequently kept constant with the perfusion pump. A total of 22 hearts were evaluated. Each heart was studied at only one flow rate, ranging from 0.3 to 3.5 mL/min/g of LV wet weight. The balloon volume and the stimulus rate remained constant throughout all experiments. After 10 min at the experimental flow rate, a mixed-isotope bolus consisting of ^{131}I -albumin (0.14 μCi), ^{18}F -FDHR (4.6 μCi), and ^{201}Tl (0.32 μCi) was injected just above the aortic cannula in 0.2 mL of perfusate buffer containing BSA but no RBCs. Venous sampling was performed as previously described (14,18).

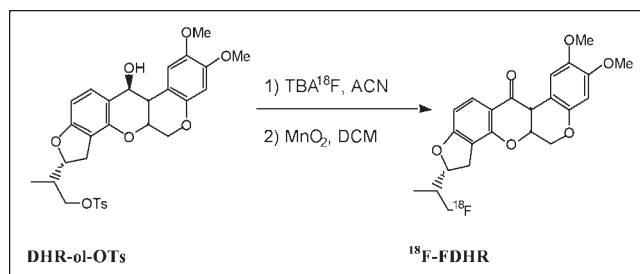
Radiopharmaceutical Agents

^{201}Tl was purchased from Mallinckrodt Medical. BSA was labeled with ^{131}I (DuPont-NEN Research Products) by use of the IODO-GEN (Pierce) protein iodination technique (19).

High-specific-activity ^{18}F was prepared by the $^{18}\text{O}(\text{p},\text{n})^{18}\text{F}$ reaction with 10-MeV protons from the LBNL Biomedical Isotope Facility CTI RDS 111 cyclotron and ^{18}O -enriched water. The aqueous ^{18}F -fluoride ion was azeotropically dried with acetonitrile (ACN) under a gentle stream of nitrogen in the presence of tetra-*n*-butyl ammonium hydroxide to form reactive tetra-*n*-butyl ammonium ^{18}F -fluoride (TBA^{18}F). Nucleophilic displacement of the tosylate moiety of 7'-tosyloxy-6',7'-dihydroroten-12-ol (DHR-ol-OTs) with the ^{18}F -fluoride ion (TBA^{18}F in acetonitrile for 20 min at 100°C) provided 7'- ^{18}F -fluoro-6',7'-dihydroroten-12-ol (^{18}F -FDHR-ol). The crude reaction mixture was filtered through a short plug of silica with ethyl acetate to remove nonreacted ^{18}F -fluoride, and the solvent was removed at 100°C under a stream of nitrogen.

^{18}F -FDHR-ol was oxidized with MnO_2 in a slurry of Celite (Celite Corp.) and dichloromethane (DCM) to provide 7'- ^{18}F -fluoro-6',7'-dihydrorotenone (^{18}F -FDHR). The reaction mixture was filtered through Celite, diluted with high-pressure liquid chromatography solvent, and purified by high-pressure liquid chromatography (Partisil M9 25 [], containing 25% ethyl acetate and 75% hexanes, at 6 mL/min). The product fraction was isolated, the solvent was removed at 100°C under a stream of nitrogen, and ethanol was added. The radiochemical purity was >99%.

The production of ^{18}F -FDHR from DHR-ol-OTs is shown in Scheme 1.



SCHEME 1. Production of ^{18}F -FDHR from DHR-ol-OTs.

RBC Uptake and Albumin Binding

Studies of the binding of ^{18}F -FDHR and ^{201}Tl to RBCs were conducted at 37°C in the presence and in the absence of BSA. The hematocrit was 21%, and the concentration of BSA was 2.2% (w/v). In the first set of experiments ($n = 3$), ^{18}F -FDHR, ^{201}Tl ,

RBCs, and BSA were incubated together in buffer. In the second set of experiments ($n = 3$), ^{18}F -FDHR and ^{201}Tl were incubated in buffer with RBCs but without BSA. Aliquots from both experimental series were removed and briefly centrifuged (15–20 s at 16,000g) to pellet the RBCs at various times (30 s–15 min) after the addition of the 2 perfusion tracers. The relative binding of ^{18}F -FDHR and ^{201}Tl to RBCs was determined by measuring counts in the cell pellet and in the supernatant (plus or minus albumin). In experiments with BSA, the minimal amount of ^{18}F -FDHR and ^{201}Tl bound to BSA was determined by precipitating BSA with trichloroacetic acid to a final concentration of 10% and measuring counts in the protein pellet and in the supernatant separately.

Data Acquisition and Data Analysis

Venous samples and aliquots of a dilution of the isotope injection solution were counted by use of a γ -counter as previously described (18). Myocardial deposition kinetics for ^{18}F -FDHR and ^{201}Tl were assessed from the measured venous sample activity. The venous sample activity was expressed as the fractional venous appearance rate, $h(t)$, and computed as follows:

$$h(t) = \frac{FC_i(t)}{Q_0}, \quad \text{Eq. 1}$$

where F denotes the blood flow (in mL/s), $C_i(t)$ denotes the venous sample activity (in cps/g), and Q_0 denotes the injected activity (in cps). Physically, $h(t)$ is a transport function that is determined by intravascular transport and dispersion in addition to bidirectional diffusion into and out of the extravascular space.

The multiple-indicator dilution technique (15) and spectral analysis (16) were used to assess blood–tissue exchange of ^{18}F -FDHR and ^{201}Tl . The fundamental assumption of the multiple-indicator dilution technique is that the intravascular reference tracer (^{131}I -albumin) accurately measures intravascular ^{18}F -FDHR and ^{201}Tl transport and dispersion. On the basis of this assumption, the differences between the ^{131}I -albumin venous concentration curve and the curves for ^{18}F -FDHR and ^{201}Tl are used to measure transit time delays attributable to movement of the 2 flow tracers into and out of the extravascular space.

Mathematic analysis was based on a linear-system approach that assumes that the distribution of transit times for all 3 tracers does not change with time, that there is no interaction between the tracer concentrations of radiolabeled reference and perfusion molecules, and that the uptake of any one perfusion tracer molecule does not influence the uptake of any other perfusion tracer molecule. With this formulation, each perfusion tracer in the venous output of the heart was modeled as a convolution of the appearance of the intravascular reference tracer with a unit impulse response function. The unit impulse response function is the diffusible tracer venous concentration curve that would be observed after an idealized bolus without circulatory dispersion or transport delay. Physically, the impulse response function measures bidirectional diffusion into and out of the extravascular space after intravascular transport and dispersion are condensed into a nondelayed, narrow spike.

Spectral analysis quantified ^{18}F -FDHR and ^{201}Tl extravascular transit time delays by producing a spectrum of kinetic components that described the unit impulse response function of each flow tracer. The impulse response function was computed by deconvolving the perfusion tracer venous concentration curves by the intravascular reference tracer (^{131}I -albumin) venous concentration curve. A nonnegative weighted least-squares algorithm was used

to model the diffusible tracer fractional venous appearance rate at time t , $h_D(t)$, as having one component that behaves like the reference tracer, $h_R(t)$, along with delayed components that can each be represented as the convolution of the reference tracer curve with a decaying exponential, as follows:

$$h_D(t) = h_R(t) \cdot i(t) \equiv \int_0^t h_R(\tau) i(t - \tau) d\tau, \quad \text{Eq. 2}$$

where $i(t)$ is the unit impulse response function, which is expressed as follows:

$$i(t) = c_0 \delta(t) + \sum_{j=1}^n \frac{c_j}{t_j} e^{-t/t_j}, \quad \text{Eq. 3}$$

where $\delta(t)$ is the Dirac delta function that yields the nondelayed component that behaves like the reference tracer. This component contains the fraction c_0 of injected activity that never escapes into the extravascular space. Through extrapolation of the spectral model to infinite time, the j th-delayed component contains a fraction c_j of the injected activity that has a mean transit delay time of t_j attributable to bidirectional diffusion between the vascular and extravascular spaces.

A total of 100 nonnegative components were used, with exponential time constants ranging between 1 s and 190 min equally spaced on a logarithmic scale. The extrapolated spectral components were not constrained to add up to 1 because of the relatively short time frame of the experiments (15 min) compared with the mean transit delay time of the slowest possible spectral component (190 min). Given m positive delayed components indexed according to increasing mean transit delay time, the first $m - 1$ components were termed intermediate components and the m th component was termed the slow component. With this kinetic model, the extraction fraction, D_0 , for a diffusible tracer is as follows:

$$D_0 = 1 - c_0, \quad \text{Eq. 4}$$

and the combined fraction and combined mean transit delay time for the intermediate components are as follows:

$$(c_{1, \dots, m-1}, t_{1, \dots, m-1}) = \left(\sum_{j=1}^{m-1} c_j, \frac{\sum_{j=1}^{m-1} c_j t_j}{\sum_{j=1}^{m-1} c_j} \right). \quad \text{Eq. 5}$$

The deconvolved net tracer retention at time t , $E_{\text{net}}(t)$, is as follows:

$$E_{\text{net}}(t) = 1 - \int_0^t i(\tau) d\tau = 1 - c_0 - \sum_{j=1}^m c_j (1 - e^{-t/t_j}). \quad \text{Eq. 6}$$

The deconvolved fractional escape rate, $\text{FER}(t)$, a measure of tracer washout, was calculated as the ratio of the delayed components of the impulse response function and $E_{\text{net}}(t)$, for $t > 0$, as follows:

$$\text{FER}(t) = \frac{i(t)}{E_{\text{net}}(t)} = \frac{\sum_{j=1}^m \frac{c_j}{t_j} e^{-t/t_j}}{1 - c_0 - \sum_{j=1}^m c_j (1 - e^{-t/t_j})}. \quad \text{Eq. 7}$$

Net tissue tracer uptake, $U(t)$, was computed as the product of tracer delivery by way of myocardial blood flow (F) and $E_{\text{net}}(t)$, as follows:

$$U(t) = F \cdot E_{\text{net}}(t). \quad \text{Eq. 8}$$

Net uptake, $U(t)$, provides a measure of extravascular tissue tracer content and is the best index of the ability of a perfusion tracer to accurately report flow; for example, for an ideal tracer with an $E_{\text{net}}(t)$ of 1 over all times and flows, $U(t)$ is equal to flow.

Statistics

Data are expressed as the mean \pm SD. Statistical analyses were performed with StatView statistical software (Abacus Concepts) and the MATLAB Statistics Toolbox (MathWorks). Regression lines were obtained with the unweighted least-squares method. A t test was used to test hypotheses about the slopes and y-intercepts of individual regression lines. Welch's procedure (20) was used to compare the slopes of regression lines and to compare the areas under uptake-versus-flow curves. Paired comparisons of kinetic parameters of ^{18}F -FDHR and ^{201}Tl were made with both a paired t test and a nonparametric Wilcoxon signed-rank test. In all cases, the 2 tests yielded similar results regarding the statistical significance of the differences, and the larger of the 2 P values is reported. A P value of <0.05 was considered statistically significant.

RESULTS

RBC and Albumin Binding

Both bovine RBCs and BSA bound ^{18}F -FDHR. In the absence of BSA, the rate with which ^{18}F -FDHR bound to RBCs was rapid; after 30 s of incubation, $90.5\% \pm 0.6\%$ of ^{18}F -FDHR was RBC associated, and this value did not change significantly over 15 min. The average value across all time points was $90.5\% \pm 0.5\%$. As with RBCs alone, the binding of ^{18}F -FDHR to RBCs in the presence of BSA was also rapid; steady-state binding was present after 30 s of incubation. However, in the presence of BSA, the binding of ^{18}F -FDHR to RBCs declined to an average across all time points of $37.7\% \pm 2.1\%$. When BSA from the RBC supernatant was precipitated with trichloroacetic acid, equilibration between free ^{18}F -FDHR and BSA-bound ^{18}F -FDHR was present after 30 s of incubation; an average of $98.9\% \pm 1.4\%$ of total ^{18}F -FDHR activity was associated with albumin.

In contrast to the ^{18}F -FDHR results, the rate with which ^{201}Tl bound to RBCs was much slower, requiring approximately 15 min (with or without BSA) to reach a constant value. The presence of BSA resulted in an initial increase in RBC-associated ^{201}Tl compared with that seen with RBCs in the absence of BSA. However, by 15 min, RBCs incubated with or without BSA reached the same levels, binding $55.2\% \pm 0.1\%$ of the total ^{201}Tl without BSA and $55.4\% \pm 0.4\%$ with BSA. Also, in contrast to the ^{18}F -FDHR results where virtually all of the ^{18}F -FDHR in the supernatant was bound to albumin at 15 min, only $47.7\% \pm 1.7\%$ of the ^{201}Tl in the supernatant was bound to albumin.

Myocardial Tracer Transport and Impulse Response Function

Figure 1A shows the concentration-time curves, expressed as fractional venous appearance rates, for ^{18}F -

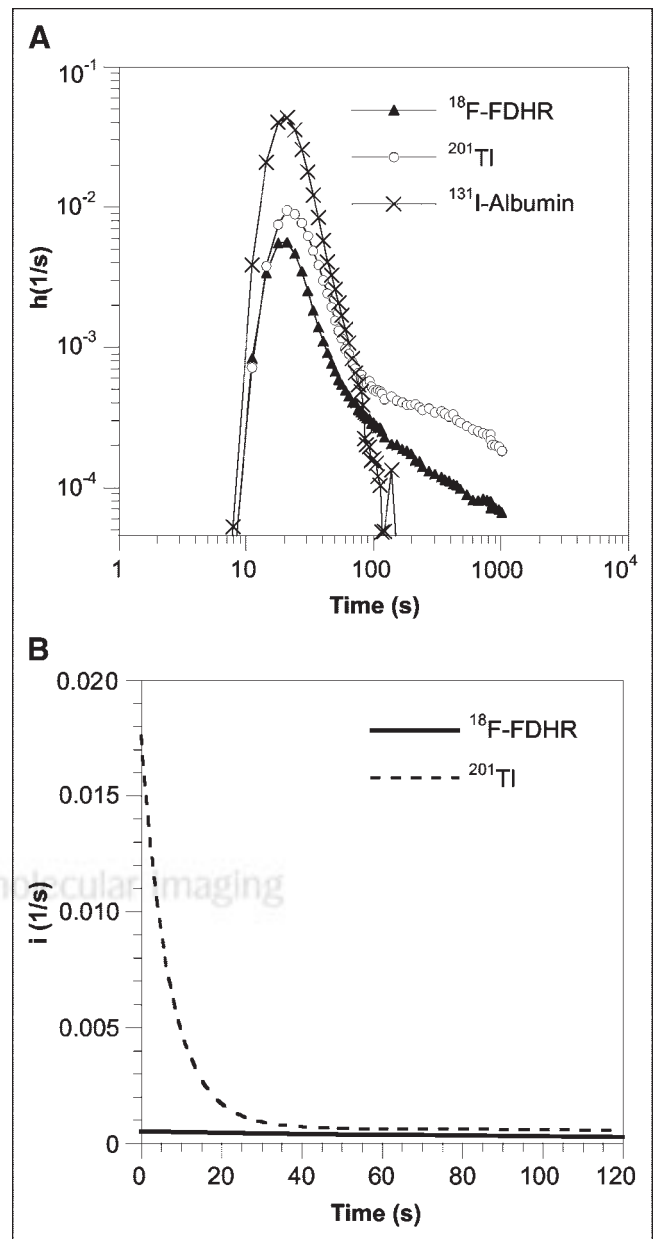


FIGURE 1. (A) Fractional venous appearance rate, $h(t)$, for ^{18}F -FDHR, ^{201}Tl , and ^{131}I -albumin as a function of venous collection times. (B) Delayed components of the deconvolved impulse response function, $i(t)$, for the first 120 s. Both datasets are from the same experiment; the coronary flow rate was 1.6 mL/min/g of LV wet weight.

FDHR, ^{201}Tl , and ^{131}I -albumin in 1 experiment. Although the 3 tracers were introduced as a compact bolus, transport through the myocardium and associated perfusion tubing resulted in considerable temporal dispersion of the tracers. For the intravascular tracer, the fractional venous appearance rates reflected the distribution of transit times through the myocardial vasculature as well as the inflow and outflow tubing. For the 2 diffusible flow tracers, some molecules remained in the vasculature with the same transit time distribution as the intravascular tracer. Other molecules

escaped into the extravascular space, where they either remained trapped for the duration of the experiment or diffused back into the vascular space. Escape of the 2 perfusion tracers from the vascular space is evident from their lower fractional venous appearance rates during the initial peak of the venous concentration curves. Subsequent reentry of the 2 perfusion tracers was seen during the later portions of the curves, when their fractional venous appearance rates exceeded that of the intravascular tracer.

The delayed components of the impulse response function for the first 2 min of this experiment are displayed in Figure 1B. These delayed components are the sum of decaying exponentials from Equation 3 and depict the distribution of transit time delays attributable to movement of the flow tracer into the extravascular space followed by back-diffusion into the intravascular space. In this experiment, a larger amount of ^{201}Tl reentered the vascular space, indicating that more extracted ^{201}Tl than $^{18}\text{F-FDHR}$ diffused out of this heart during the first 120 s after tracer introduction.

The nondelayed component fractions, c_0 (Eq. 3), of the impulse response function for this experiment were 0.13 for $^{18}\text{F-FDHR}$ and 0.14 for ^{201}Tl (data not shown). These were the fractions of flow tracer molecules that remained inside the vasculature with transit time distributions indistinguishable from that of ^{131}I -albumin.

Spectral Analysis

As was the case with previously reported spectral analyses of data for ^{125}I -iodorotone and $^{99\text{m}}\text{Tc}$ -sestamibi (14), there was consistency between measured and modeled fractional venous appearance curves for $^{18}\text{F-FDHR}$ and ^{201}Tl . Modeled diffusible tracer fractional venous appearance curves were obtained by convolving the measured ^{131}I -albumin reference curve with the impulse response function given by the spectral models. The average root-mean-square differences between measured and modeled data were nor-

malized to the root-mean-square values for measured data and expressed as percentages. For the 22 experiments, these differences averaged $9.7\% \pm 6.0\%$ for $^{18}\text{F-FDHR}$ and $3.1\% \pm 2.6\%$ for ^{201}Tl .

A second similarity to previously reported data (14) was that some spectral model parameters exhibited variability (Table 1). The number of delayed components in the impulse response function ranged from 1 to 4 for $^{18}\text{F-FDHR}$ and from 2 to 5 for ^{201}Tl . For each experiment, the number of $^{18}\text{F-FDHR}$ components was less than or equal to the number of ^{201}Tl components. On average, $^{18}\text{F-FDHR}$ models contained 3.3 delayed components and ^{201}Tl models contained 4.3 delayed components. However, despite this variability, robust estimates of extraction fraction, net retention, and washout (Eqs. 4, 6, and 7, respectively) were obtained by evaluating the impulse response function (Eq. 3) and its integral.

Two notable trends in the spectra were that the combined fraction of intermediate components, $c_{1,\dots,m-1}$, was significantly smaller for $^{18}\text{F-FDHR}$ than for ^{201}Tl ($P < 0.002$) and that the slow-component mean transit delay time, t_m , was significantly greater for $^{18}\text{F-FDHR}$ than for ^{201}Tl ($P < 0.002$). Thus, the results obtained with the spectral model indicated that less $^{18}\text{F-FDHR}$ washed out in the 1- to 3-min intermediate time frame and that the long-term retention of $^{18}\text{F-FDHR}$ was also better.

$^{18}\text{F-FDHR}$ and ^{201}Tl Extraction

Figure 2 shows the initial extraction fraction (Eq. 4) values for $^{18}\text{F-FDHR}$ and ^{201}Tl as a function of myocardial blood flow for all 22 experiments. Over the range of flows evaluated, there was no significant difference between the mean \pm SD initial extraction fraction values for $^{18}\text{F-FDHR}$ (0.85 ± 0.07) and ^{201}Tl (0.87 ± 0.05) ($P > 0.1$). The initial extraction fraction for $^{18}\text{F-FDHR}$ decreased with flow ($P <$

TABLE 1
Spectral Analysis Components for $^{18}\text{F-FDHR}$ and ^{201}Tl

Tracer	Percentile	Value for the following component:				
		Nondelayed (c_0)	Intermediate		Slow	
			$c_{1,\dots,m-1}$	$t_{1,\dots,m-1}$	c_m	t_m
$^{18}\text{F-FDHR}$	75	0.20	0.14	3.7	1.1	190*
$^{18}\text{F-FDHR}$	50	0.14	0.11	2.8	0.55	190*
$^{18}\text{F-FDHR}$	25	0.09	0.09	2.0	0.31	82
^{201}Tl	75	0.17	0.39	3.8	0.95	130
^{201}Tl	50	0.14	0.24	0.92	0.64	28
^{201}Tl	25	0.08	0.19	0.19	0.56	19

*Slow component has artificial upper limit imposed by spectral analysis, which fitted components having mean transit delay times ranging from 1 s to 190 min.

Data represent upper quartile, median, and lower quartile values (75th, 50th, and 25th percentiles) for fractions and mean transit delay times for spectral model impulse response components for 22 experiments. Fractions and mean transit delay times for intermediate components were combined by use of Equation 5. Fractions c_0 , $c_{1,\dots,m-1}$, and c_m are dimensionless. Mean transit delay times $t_{1,\dots,m-1}$ and t_m are reported in minutes.

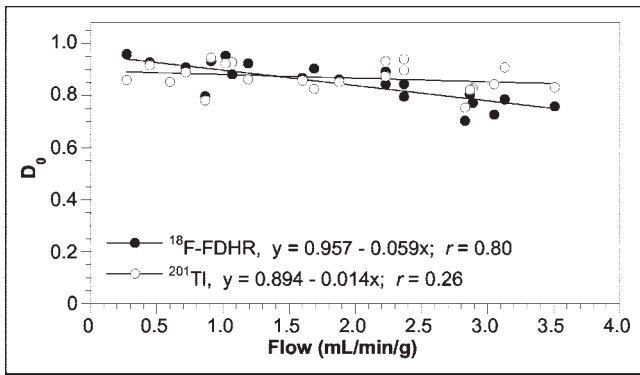


FIGURE 2. Initial extraction fractions, D_0 , for ^{18}F -FDHR and ^{201}Tl as a function of blood flow. Data were pooled from 22 experiments; each data point represents a single experiment. Equations for the linear fits to the data points are shown.

0.0001), whereas flow did not have a significant effect on the initial extraction fraction for ^{201}Tl ($P > 0.2$).

^{18}F -FDHR and ^{201}Tl Washout

Figure 3 is a 3-dimensional illustration (surface plot) of the effects of both time and flow on ^{18}F -FDHR and ^{201}Tl washout as quantified by FER(t) (Eq. 7). The surface heights represent the FER(t) values for ^{18}F -FDHR (Fig. 3A and 3C) and ^{201}Tl (Fig. 3B and 3D). The lines parallel to the flow axis depict the effect of flow on FER(t) at only 1 point in time. These lines were obtained from linear regressions of FER(t) values generated by evaluating Equation 7 at selected time points with data from all 22 experiments. The lines parallel to the time axis depict the effect of time on FER(t) at only 1 coronary flow. These lines were obtained

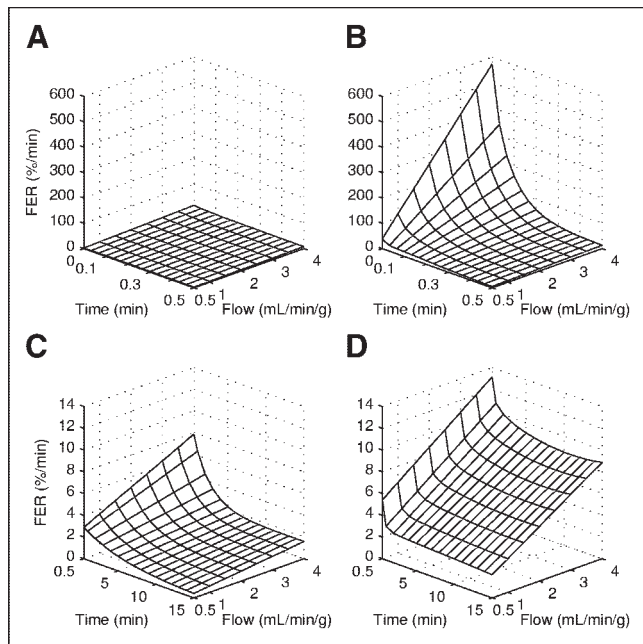


FIGURE 3. FER(t) as a function of flow and time for ^{18}F -FDHR (A and C) and ^{201}Tl (B and D) during the first 30 s (A and B) and from 30 s to 15 min (C and D).

by connecting points on the regression lines for FER(t) versus flow.

Figures 3A and 3B show the effects of time and flow on ^{18}F -FDHR and ^{201}Tl FER(t) values during the first 30 s after tracer introduction. The surfaces are composed of 16 regression lines for FER(t) versus flow obtained at 2-s increments. FER(t) values for ^{201}Tl were much higher than those for ^{18}F -FDHR over all flows during the initial 30 s ($P < 0.0001$ for each time point). For both tracers, increasing flow resulted in higher FER(t) values for each point in time ($P < 0.02$ and $P < 0.002$ for ^{18}F -FDHR and ^{201}Tl , respectively). When flow was kept constant, there was a reduction in ^{201}Tl and ^{18}F -FDHR FER(t) values with time because of decreasing washout of activity from intermediate spectral components. ^{201}Tl washout was very rapid at high flows early after tracer introduction. At low flows and after 15–20 s, the effects of time and flow were less prominent. Flow exerted a much stronger effect on ^{201}Tl FER(t) than on that of ^{18}F -FDHR during the first 20 s ($P < 0.05$ for each time point).

Figures 3C and 3D show surfaces composed of 16 regression lines for FER(t) versus flow obtained at 30 s and at 1-min increments from 1 to 15 min. As was the case during the first 30 s, FER(t) values for ^{201}Tl were higher than those for ^{18}F -FDHR ($P < 0.001$ for each time point). Although less striking than immediately after isotope introduction, flow had a stronger effect on ^{201}Tl FER(t) than on that of ^{18}F -FDHR ($P < 0.05$ for each time point). Reflecting this difference, increasing flow rates increased ^{201}Tl FER(t) values at all time points ($P < 0.001$ for each time point), whereas ^{18}F -FDHR values were only intermittently increased (significant increases from 30 s to 3 min and from 7 to 15 min [$P < 0.05$ for each time point]). When flow was kept constant, ^{18}F -FDHR and ^{201}Tl FER(t) values declined with time because of decreasing washout of activity associated with intermediate spectral components.

^{18}F -FDHR and ^{201}Tl Retention

Figure 4 is a surface plot of the effects of time and flow on ^{18}F -FDHR and ^{201}Tl net retention; its configuration is similar to that of Figure 3, except that the flow axis has been reversed to allow better visualization of the effect of flow on

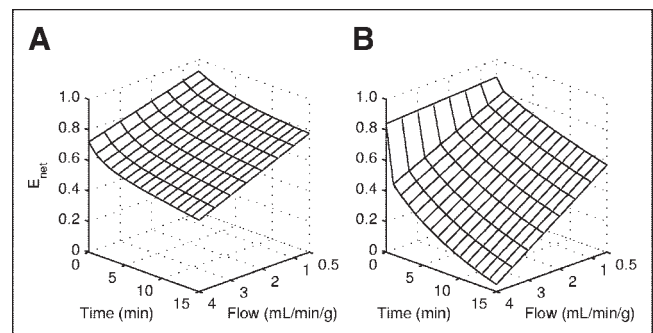


FIGURE 4. $E_{\text{net}}(t)$ as a function of flow and time for ^{18}F -FDHR (A) and ^{201}Tl (B).

tracer retention. The 16 lines parallel to the flow axis are linear regression lines obtained for E_{net} values from all 22 experiments by evaluating Equation 6 at 1-min increments. For both ^{18}F -FDHR and ^{201}Tl , the regression lines at time = 0 min are identical to the lines in Figure 2 and indicated that flow had a stronger effect on ^{18}F -FDHR initial extraction fraction than on ^{201}Tl initial extraction fraction. For all subsequent time points, ^{18}F -FDHR net retention was higher than that for ^{201}Tl ($P < 0.0001$ for each time point), because of the higher FER(t) values for ^{201}Tl . Increasing coronary flow reduced both ^{18}F -FDHR net retention and ^{201}Tl net retention ($P < 0.0001$ for each tracer for each time point). Consistent with the different sensitivities to the effects of flow on washout, the decline for ^{201}Tl was steeper than that for ^{18}F -FDHR along the flow axis at times of ≥ 1 min, indicating that flow had a greater effect on ^{201}Tl net retention ($P < 0.05$ for each time point).

^{18}F -FDHR and ^{201}Tl Uptake

Figure 5 is a surface plot of the effects of time and flow on ^{18}F -FDHR and ^{201}Tl net uptake. The direction of the flow axis is identical to that in Figure 3. Because net uptake is computed as the product of flow and E_{net} (Eq. 8), ideal flow tracers have an E_{net} of 1 at all times and flows. For such ideal perfusion tracers, this surface plot would reduce to a 2-dimensional graph with flow and net uptake values falling on the line of identity. As shown in Figures 2 and 4, neither ^{18}F -FDHR nor ^{201}Tl had an initial extraction fraction of 1 at any flow, and the net retention of both tracers declined with increasing time and flow. When the 2 agents were compared, initial ^{18}F -FDHR uptake values were less linearly related to flow than those for ^{201}Tl , because the initial extraction of ^{18}F -FDHR was sensitive to flow and the initial extraction of ^{201}Tl was not (Fig. 2). However, ^{201}Tl retention dropped sharply during the first minute and was more sensitive to flow than ^{18}F -FDHR retention for the remainder of the 15-min experiment (Fig. 4). (At later times, ^{201}Tl uptake actually declined as flow increased because of accelerated tracer washout at high flows in the absence of ^{201}Tl recirculation, a condition not encountered in vivo). Thus, after the first minute, ^{18}F -FDHR net uptake values were higher and more linearly related to flow than those for ^{201}Tl .

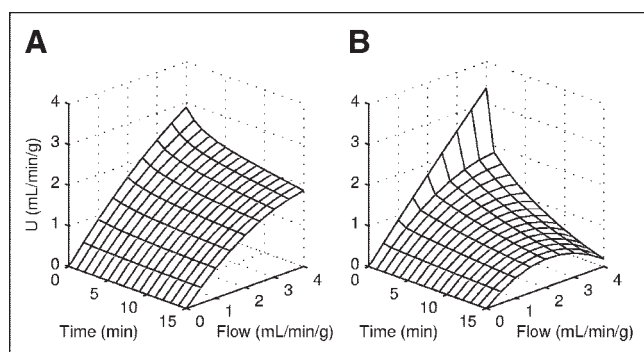


FIGURE 5. Net uptake, $U(t)$, as a function of flow and time for ^{18}F -FDHR (A) and ^{201}Tl (B).

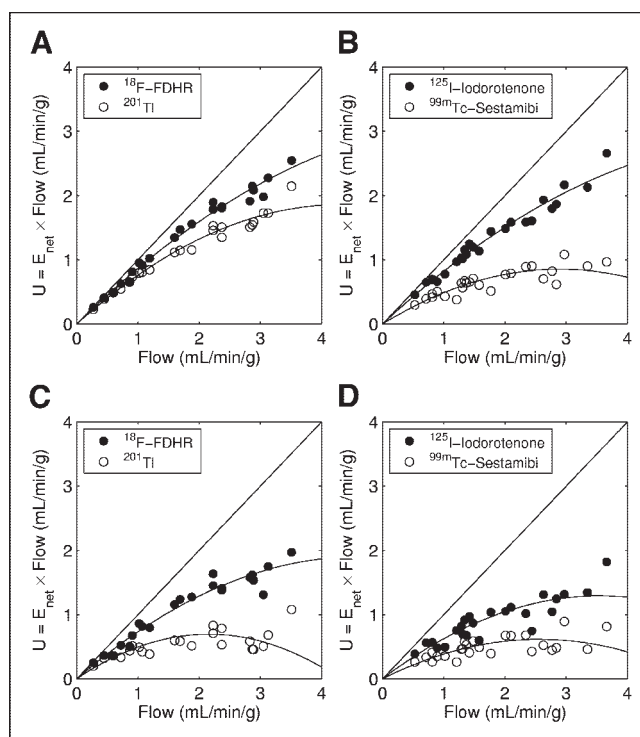


FIGURE 6. Relationship between net uptake, $U(t)$, and flow for ^{18}F -FDHR and ^{201}Tl (A and C) and ^{125}I -iodoroteronone and $^{99\text{m}}\text{Tc}$ -sestamibi (B and D) at 1 min (A and B) and 15 min (C and D).

Figure 6 shows the relationship between net uptake and flow at 1 and 15 min after tracer introduction for ^{18}F -FDHR and ^{201}Tl from the present study and comparable values for ^{125}I -iodoroteronone and $^{99\text{m}}\text{Tc}$ -sestamibi from a previous investigation (14). The results for ^{18}F -FDHR and ^{201}Tl are shown in Figures 6A and 6C, and those for ^{125}I -iodoroteronone and $^{99\text{m}}\text{Tc}$ -sestamibi are shown in Figures 6B and 6D. When the areas under the uptake-versus-flow curves at 1 min were compared (Figs. 6A and 6B), the net uptake values for both ^{18}F -FDHR and ^{125}I -iodoroteronone were closer to the line of identity than those for either of the clinically available tracers ($P < 0.0001$ for each comparison). There was a small but statistically significant difference in the areas under the uptake-versus-flow curves for the 2 radiolabeled rotenone analogs at 1 min after tracer injection, with net uptake values for ^{18}F -FDHR being slightly closer to the line of identity than those for ^{125}I -iodoroteronone ($P < 0.05$).

At 15 min after the injection of the isotopes (Figs. 6C and 6D), the net uptake values for the 2 radiolabeled rotenone analogs remained closer to the line of identity than those of either ^{201}Tl or $^{99\text{m}}\text{Tc}$ -sestamibi ($P < 0.0001$ for each comparison). When ^{125}I -iodoroteronone and ^{18}F -FDHR were compared, the differences in the areas under the uptake-versus-flow curves were slightly larger than those at 1 min, with net uptake values for ^{18}F -FDHR continuing to be closer to the line of identity than those for ^{125}I -iodoroteronone ($P < 0.001$). These results indicate that both ^{18}F -FDHR and ^{125}I -iodoroteronone were better flow tracers than either ^{201}Tl or $^{99\text{m}}\text{Tc}$ -

sestamibi from 1 to 15 min after bolus tracer introduction into the isolated rabbit heart. In addition, ^{18}F -FDHR was a slightly better flow tracer than ^{125}I -iodorotene over the same time interval.

DISCUSSION

We compared ^{18}F -FDHR, a radiolabeled rotenone analog, and ^{201}Tl as myocardial perfusion indicators in the isolated rabbit heart. We observed that ^{18}F -FDHR tissue tracer content was more closely related to flow than ^{201}Tl content, except for a single measurement immediately after tracer introduction. Similarly, in previous work, we observed that the tissue tracer content of another radiolabeled rotenone analog, ^{125}I -iodorotene, was more closely related to flow than that of $^{99\text{m}}\text{Tc}$ -sestamibi (14). When results from the 2 studies were combined, both ^{18}F -FDHR and ^{125}I -iodorotene tissue tracer contents were more closely related to flow than either ^{201}Tl or $^{99\text{m}}\text{Tc}$ -sestamibi tissue tracer content. These observations indicate that ^{18}F -FDHR and ^{125}I -iodorotene are better flow tracers than ^{201}Tl and $^{99\text{m}}\text{Tc}$ -sestamibi in the isolated rabbit heart.

RBC and Albumin Binding and Permeation of Capillary Wall

The initial extraction fraction of a tracer is frequently used to assess its ability to permeate the capillary wall (21). Usually, neutral lipophilic compounds readily escape from the capillary into the extravascular space, because these compounds can diffuse through endothelial cell membranes (5). However, the initial extraction fraction for ^{18}F -FDHR was no higher than that for ^{201}Tl , a charged molecule that diffuses primarily through pores in the capillary wall (5). In addition, changes in flow affected ^{18}F -FDHR initial extraction fraction but failed to significantly alter ^{201}Tl initial extraction fraction. Because ^{18}F -FDHR binding to RBCs and albumin was virtually complete after 30 s of incubation, the most plausible explanation for these observations is that the rate-limiting step for ^{18}F -FDHR permeation of the capillary wall was dissociation from albumin or diffusion from RBCs.

Although infrequently cited in the cardiac literature, the binding of ^{201}Tl to RBCs has been extensively investigated (22–24); it is well established that thallium enters the intracellular space of RBCs and may not be available for exchange with the myocardium (25). In the present study, we observed that ^{201}Tl entered bovine RBCs slowly relative to ^{18}F -FDHR; 55% was associated with the red cell fraction at 15 min. These observations are consistent with experience with ^{201}Tl in the RBC-perfused rabbit heart. In a study comparing ^{201}Tl with $^{99\text{m}}\text{Tc}$ (26), Marshall et al. observed that the peak extraction fraction for ^{201}Tl was 0.83 ± 0.06 , a value similar to that observed in this investigation. In these 2 studies, the isotope injection solution did not contain RBCs. However, in another investigation (18), the initial extraction fraction for ^{201}Tl was only 0.67 ± 0.07 . In this latter study, the injection solution contained RBCs. Because

there was usually a lag time of up to 15 min between the addition of ^{201}Tl to the RBC-containing perfusate and injection, there was sufficient time for ^{201}Tl to enter RBCs and be unavailable to the myocardium. Because this phenomenon has not been investigated in vivo, the effect of red cell sequestration on regional ^{201}Tl distribution or redistribution in patients is not clear.

Because ^{201}Tl is charged, it has limited capillary permeability and is better extracted at low flows than at high flows (21,27–29). However, in both the current investigation and a previously published report (18), the expected decline in the thallium initial extraction fraction was not observed at higher coronary flows. There are 2 potential explanations for this anomalous behavior. First, at low flows, it takes longer to travel from the point of injection to myocardial capillaries, so that there is increased time for thallium to be sequestered inside RBCs. Because thallium inside RBCs is not available to the myocardium, the expected increase in the extraction fraction at low flows is not observed. Second, capillary permeability could increase as flow is increased because of either capillary recruitment or a temporal change in the capillary “twinkling” pattern, both obviating a decline in the extraction fraction at high flows. Weich et al. (29) observed an apparent increase in capillary permeability at higher flows when cardiac work was increased by rapid atrial pacing.

Washout and Retention

The ability to separate intravascular tracer distribution from extravascular tracer distribution by spectral analysis allows a qualitative comparison of the rate-limiting steps of ^{18}F -FDHR versus ^{201}Tl exchange between the blood and the myocardium. Early FER(t) provides a measure of the fraction of initially extracted tracer that backdiffuses into the intravascular space. In these experiments, early FER(t) for ^{201}Tl was much higher than that for ^{18}F -FDHR. Since the rates of diffusion from capillaries were similar for these 2 tracers, the higher backdiffusion of ^{201}Tl is consistent with diminished sarcolemmal permeability for ^{201}Tl . When this information is combined with the blood component binding studies and the 2 tracers are compared, the data suggest that the diffusion of ^{18}F -FDHR into myocytes is limited by dissociation from RBCs or albumin, whereas that of ^{201}Tl is limited by sarcolemmal permeability.

At late times in these experiments, the escape of these 2 flow tracers was related mostly to diffusion from the intracellular space. As with early FER(t), more ^{201}Tl than ^{18}F -FDHR escaped from the myocardium. Reflecting the less effective intracellular sequestration, ^{201}Tl retention was lower and more affected by flow than ^{18}F -FDHR retention at all times after the first measurement.

Although the superior retention of ^{18}F -FDHR is presumably related to abundant mitochondria in the myocardium (10–13), the intracellular binding characteristics of ^{18}F -FDHR (and ^{125}I -iodorotene) have not been systematically evaluated in the heart. In addition, the effects of changes in

the mitochondrial metabolic rate attributable to altered workload, substrate supply, and ischemia are unknown. It is quite possible that extraction and retention of the radiolabeled rotenone analogs are altered by changes in mitochondrial function, limiting their use as flow tracers.

Comparison to Other Positron-Emitting Flow Tracers

Three positron-emitting flow tracers are currently available for clinical use. ^{82}Rb is a generator-produced deposited flow tracer that does not require an on-site cyclotron. However, the use of ^{82}Rb has been limited because it has a short half-life (75 s) and a high endpoint energy that degrades image quality. Also, the kinetics of ^{82}Rb myocardial deposition indicate that it is not as good a flow tracer as ^{201}Tl (18). In contrast to ^{82}Rb , ^{15}O -water is a flow-limited tracer; myocardial tracer delivery and washout are determined by the rate of coronary flow. Qualitative estimation of regional perfusion is not possible from a single image; to estimate flow with ^{15}O -water, dynamic image acquisition is required, and quantification of regional flow requires a tracer kinetic model.

^{13}N -Ammonia is a deposited flow tracer that was initially used clinically to assess regional blood flow in 1972 (30) and has been shown to provide accurate qualitative assessment of regional myocardial perfusion directly from tomographic images (31). ^{13}N -Ammonia has also been used to quantify regional flow (32–37), although the rapid appearance of ^{13}N -containing metabolites makes accurate assessment of the input function difficult. Previous studies evaluating ^{13}N -ammonia kinetics in vitro did not use the multiple-indicator dilution technique (38), making comparison to the current results nonproductive.

^{18}F -FDHR has 2 advantages over the positron-emitting flow tracers currently in use. First, both ^{15}O -water and ^{13}N -ammonia have short half-lives (2 and 10 min, respectively) and require an on-site cyclotron. ^{18}F has a longer half-life (110 min) and does not require an on-site cyclotron; it can be obtained commercially. Second, ^{18}F has the potential of providing excellent image resolution relative to ^{82}Rb .

CONCLUSION

The results of this study and a previous investigation (14) have shown ^{18}F -FDHR and ^{125}I -iodorotenone to be superior flow tracers relative to ^{201}Tl and $^{99\text{m}}\text{Tc}$ -sestamibi in the isolated rabbit heart. Although it is likely that these mitochondrion-avid tracers will be trapped in the myocardium of most mammalian species, there are issues that need further investigation. The first is that blood component binding in patients may be different from that in bovine RBCs and albumin. The second issue relates to potential changes in myocardial deposition when mitochondrial function is altered because of changes in workload, substrate supply, or the development of ischemia. Although these issues need to be addressed, the clear superiority of ^{18}F -FDHR and ^{125}I -iodorotenone over the tracers currently in use in the isolated

rabbit heart provides sufficient motivation to continue to evaluate rotenone analogs both in vitro and in vivo.

ACKNOWLEDGMENTS

This study was supported by National Heart, Lung, and Blood Institute grants PO1 HL25840 and RO1 HL6087701 and by the Director, Office of Science, Office of Biological and Environmental Research (OBER), Medical Science Division, U.S. Department of Energy, under OBER contract DE-AC03-76SF00098.

REFERENCES

1. Shaw LJ, Iskandrian AE, Hachamovitch R, et al. Evidence-based risk assessment in noninvasive imaging. *J Nucl Med.* 2001;42:1424–1436.
2. Iskander S, Iskandrian AE. Risk assessment using single-photon emission computed tomographic technetium-99m sestamibi imaging. *J Am Coll Cardiol.* 1998;32:57–62.
3. Gibbons RJ, Chatterjee K, Daley J, et al. ACC/AHA/ACP-ASIM guidelines for the management of patients with chronic stable angina: a report of the American College of Cardiology/American Heart Association Task Force on Practice Guidelines (Committee on Management of Patients with Chronic Stable Angina). *J Am Coll Cardiol.* 1999;33:2092–2197.
4. Alpert JS. Defining myocardial infarction: “will the real myocardial infarction please stand up?” *Am Heart J.* 2003;146:377–379.
5. Bassingthwaite JB, Raymond GM, Chan JJ. Principles of tracer kinetics. In: Zaret BL, Beller GA, eds. *Nuclear Cardiology: State of the Art and Future Directions.* St. Louis, MO: Mosby-Year Book; 1993:3–23.
6. Yoshinaga K, Katoh C, Noriyasu K, et al. Reduction of coronary flow reserve in areas with and without ischemia on stress perfusion imaging in patients with coronary artery disease: a study using oxygen 15-labeled water PET. *J Nucl Cardiol.* 2003;10:275–283.
7. Bergmann SR, Fox KA, Rand AL, et al. Quantification of regional myocardial blood flow in vivo with H_2^{15}O . *Circulation.* 1984;70:724–733.
8. Bergmann SR, Herrero P, Markham J, Weinheimer CJ, Walsh MN. Noninvasive quantitation of myocardial blood flow in human subjects with oxygen-15-labeled water and positron emission tomography. *J Am Coll Cardiol.* 1989;14:639–652.
9. Araujo LI, Lammertsma AA, Rhodes CG, et al. Noninvasive quantification of regional myocardial blood flow in coronary artery disease with oxygen-15-labeled carbon dioxide inhalation and positron emission tomography. *Circulation.* 1991;83:875–885.
10. Ueno H, Miyoshi H, Ebisui K, Iwamura H. Comparison of the inhibitory action of natural rotenone and its stereoisomers with various NADH-ubiquinone reductases. *Eur J Biochem.* 1994;225:411–417.
11. Ueno H, Miyoshi H, Inoue M, Niidome Y, Iwamura H. Structural factors of rotenone required for inhibition of various NADH-ubiquinone oxidoreductases. *Biochim Biophys Acta.* 1996;1276:195–202.
12. Greenamyre JT, Higgins DS, Eller RV. Quantitative autoradiography of dihydrorotenone binding to complex I of the electron transport chain. *J Neurochem.* 1992;59:746–749.
13. Ramsay RR, Krueger MJ, Youngster SK, Gluck MR, Casida JE, Singer TP. Interaction of 1-methyl-4-phenylpyridinium ion (MPP⁺) and its analogs with the rotenone/piercidin binding site of NADH dehydrogenase. *J Neurochem.* 1991;56:1184–1190.
14. Marshall RC, Powers-Risius P, Reutter BW, et al. Kinetic analysis of ^{125}I -iodorotenone as a deposited myocardial flow tracer: comparison with $^{99\text{m}}\text{Tc}$ -sestamibi. *J Nucl Med.* 2001;42:272–281.
15. Chinnard FP, Vosburgh GJ, Enns T. Transcapillary exchange of water and of other substances in certain organs of the dog. *Am J Physiol.* 1955;183:221–234.
16. Cunningham VJ, Jones T. Spectral analysis of dynamic PET studies. *J Cereb Blood Flow Metab.* 1993;13:15–23.
17. Marshall RC. Correlation of contractile dysfunction with oxidative energy production and tissue high energy phosphate stores during partial coronary flow disruption in rabbit heart. *J Clin Invest.* 1988;82:86–95.
18. Marshall RC, Taylor SE, Powers-Risius P, et al. Kinetic analysis of rubidium and thallium as deposited myocardial blood flow tracers in isolated rabbit heart. *Am J Physiol.* 1997;272:H1480–H1490.
19. Millar WT, Smith JFB. Protein iodination using IODO-GEN. *Int J Appl Radiat Isot.* 1983;34:639–641.
20. Kendall M, Stuart A. *The Advanced Theory of Statistics.* New York, NY: Oxford University Press; 1979.

21. Bassingthwaighe JB, Goresky CA. Modeling in the analysis of solute and water exchange in the microvasculature. In: Renkin EM, Michel CC, eds. *Handbook of Physiology*. Section 2. *The Cardiovascular System*. Vol IV. *The Microcirculation*. Bethesda, MD: American Physiological Society; 1984:549–626.
22. Sands H, Delano ML, Camin LL, Gallagher BM. Comparison of the transport of $^{42}\text{K}^+$, $^{22}\text{Na}^+$, $^{201}\text{Tl}^+$, and $^{99m}\text{Tc}(\text{dmpe})_2 \times \text{Cl}_2^+$ using human erythrocytes. *Biochim Biophys Acta*. 1985;812:665–670.
23. Skulskii IA, Manninen V. Effect of membrane potential on the passive transport of Tl^+ in human red blood cells. *Acta Physiol Scand*. 1981;111:343–348.
24. Skulskii IA, Manninen V, Glasunov VV. Thallium and rubidium permeability of human and rat erythrocyte membrane. *Gen Physiol Biophys*. 1990;9:39–44.
25. Goresky CA, Bach GG, Nadeau BE. Red cell carriage of label. *Circ Res*. 1975;36:328–351.
26. Marshall RC, Leidholdt EM Jr, Zhang DY, Barnett CA. Technetium-99m hexakis 2-methoxy-2-isobutyl isonitrile and thallium-201 extraction, washout, and retention at varying coronary flow rates in rabbit heart. *Circulation*. 1990;82:998–1007.
27. Bassingthwaighe J, Winkler B, King R. Potassium and thallium uptake in dog myocardium. *J Nucl Med*. 1997;38:264–274.
28. Melin JA, Becker LC. Quantitative relationship between global left ventricular thallium uptake and blood flow: effects of propranolol, ouabain, dipyridamole, and coronary artery occlusion. *J Nucl Med*. 1986;27:641–652.
29. Weich HF, Strauss HW, Pitt B. The extraction of thallium-201 by the myocardium. *Circulation*. 1977;56:188–191.
30. Harper PV, Lathrop KA, Krizek H, Lembares N, Stark V, Hoffer PB. Clinical feasibility of myocardial imaging with $^{13}\text{NH}_3$. *J Nucl Med*. 1972;13:278–280.
31. Schelbert HR, Wisenberg G, Phelps ME, et al. Noninvasive assessment of coronary stenoses by myocardial imaging during pharmacologic coronary vasodilation. VI: detection of coronary artery disease in human beings with intravenous N-13 ammonia and positron computed tomography. *Am J Cardiol*. 1982;49:1197–1207.
32. Hutchins GD, Schwaiger M, Rosenspire KC, Krivokapich J, Schelbert H, Kuhl DE. Noninvasive quantification of regional blood flow in the human heart using N-13 ammonia and dynamic positron emission tomographic imaging. *J Am Coll Cardiol*. 1990;15:1032–1042.
33. Krivokapich J, Smith GT, Huang SC, et al. ^{13}N Ammonia myocardial imaging at rest and with exercise in normal volunteers: quantification of absolute myocardial perfusion with dynamic positron emission tomography. *Circulation*. 1989;80:1328–1337.
34. Kuhle WG, Parenta G, Huang SC, et al. Quantification of regional myocardial blood flow using ^{13}N -ammonia and reoriented dynamic positron emission tomographic imaging. *Circulation*. 1992;86:1004–1017.
35. Beanlands RS, deKemp R, Scheffel A, et al. Can nitrogen-13 ammonia kinetic modeling define myocardial viability independent of fluorine-18 fluorodeoxyglucose? *J Am Coll Cardiol*. 1997;29:537–543.
36. Muzik O, Beanlands RS, Hutchins GD, Mangner TJ, Nguyen N, Schwaiger M. Validation of nitrogen-13-ammonia tracer kinetic model for quantification of myocardial blood flow using PET. *J Nucl Med*. 1993;34:83–91.
37. Gerber BL, Melin JA, Bol A, et al. Nitrogen-13-ammonia and oxygen-15-water estimates of absolute myocardial perfusion in left ventricular ischemic dysfunction. *J Nucl Med*. 1998;39:1655–1662.
38. Krivokapich J, Huang SC, Phelps ME, MacDonald NS, Shine KI. Dependence of $^{13}\text{NH}_3$ myocardial extraction and clearance on flow and metabolism. *Am J Physiol*. 1982;242:H536–H542.

